Journal of Solid State Chemistry **165,** 193–198 (2002)
doi:10.1006/jssc.2001.9526, available online at http://www.idealibrary.com on IDEAL®

Rapid Synthesis of Nanocrystalline TiO_2/SnO_2 Binary Oxides and Their Photoinduced Decomposition of Methyl Orange

Juan Yang, Dan Li, Xin Wang,[1] XuJie Yang, and LuDe Lu

Materials Chemistry Laboratory, Center of Nanoscience and Nanotechnology, Nanjing University of Science and Technology, Nanjing 210094, People's Republic of China

Received October 7, 2001

A rapid and simple method, the so-called stearic acid method (SAM) was developed to prepare nanostructured TiO_2/SnO_2 binary oxides by combustion of stearic acid precursors. The preparative process was studied by Fourier transform infrared spectroscopy (FT-IR). During the preparative process, metal precursors were dispersed in stearic acid at molecular level. Microstructure of the samples was investigated by X-ray diffraction (XRD), transmission electron microscopy (TEM), BET specific surface area measurement and the results were compared with those obtained by conventional sol–gel method. The photocatalytic decomposition of methyl orange was used as a model system to determine the relative influences of the preparation method and the concentration of SnO_2 on the photocatalytic activities. It was found that preparative methods affected the crystalline structure of TiO_2/SnO_2 powders and the anatase phase of TiO_2 was stabilized by the addition of SnO_2 in SAM. The samples prepared by SAM showed better dispersity, larger specific surface area and the TiO_2/SnO_2 (r=0.15, SAM) catalyst showed higher photocatalytic activity than Degussa P25.

Key Words: **stearic acid method; TiO_2/SnO_2 binary oxides; microstructure; photodegradation.**

INTRODUCTION

From the viewpoint of air and water purification, semiconductor photocatalyst TiO_2 has recently received wide interest due to its powerful oxidation strength, high photostability and nontoxicity (1–4). Properties influencing the photocatalytic activity of TiO_2 particles have been suggested to include the surface area, crystallinity, crystallite size and crystal structure (1, 5). For TiO_2, there are three polymorphs, anatase, rutile and brookite. It has been generally accepted that the anatase phase is the most active as a photocatalyst, and the high crystallinity and large specific surface area will also improve the photoactivity (6, 7).

[1] To whom correspondence should be addressed. Fax: (+86)025-4315518. E-mail: wxin@public 1.ptt.js.cn

Photoexcitation of TiO_2 with light as energy that matches its band gap yields electron–hole pairs. The photocatalytic efficiency depends on the ratio of the surface charge carrier transfer rate to the electron–hole recombination rate. Photocatalytic enhancement has been demonstrated using coupled semiconductor to suppress the recombination of photogenerated charge carriers (8–13). Coupled semiconductor TiO_2/SnO_2 has been widely studied and has been proved to be a good photocatalyst owing to its high quantum yield. The different conduction band of SnO_2 and TiO_2 results in the efficient separation of photoinduced electron–hole pair (14–16).

Usually, the sol–gel method, which involves the hydrolysis and condensation of alkoxide precursors, has been widely used for the preparation of multicomponent oxides (16–20). But it is unsuitable for preparing TiO_2/SnO_2 photocatalyst because the addition of SnO_2 will decrease the crystallinity and improve the anatase to rutile ($A \rightarrow R$) transformation of TiO_2 crystalline (5), which deteriorates the photoactivity of TiO_2/SnO_2 binary oxides. Furthermore, the sol–gel method is too time consuming because the gelation process usually needs several days or even months.

We previously found that stearic acid method was a versatile and convenient route for preparing nanostructured complex oxides (21–23). Herein, we report that this method is also convenient for preparing TiO_2/SnO_2 nanocrystalline binary oxides with anatase structure, high crystallinity, large surface area and high photocatalytic activity.

EXPERIMENTAL

Tetrabutyl titanate [$Ti(O–Bu)_4$] and hydrous stannic chloride ($SnCl_4 \cdot 5H_2O$) were used as the precursors of titania and stannic oxide, respectively. Stearic acid ($C_{17}H_{35}COOH$) was used as the solvent and dispersant. The molar ratio of these reactants was: $Ti(O–Bu)_4$: $C_{17}H_{35}COOH$: $SnCl_4 \cdot 5H_2O = 1:2:r$ ($r = 0$, 0.05, 0.10, 0.15, 0.20, 0.25).

0022-4596/02 $35.00

Firstly, half of the prescribed stearic acid was heated and melted, into which a given amount of $SnCl_4 \cdot 5H_2O$ was added. This mixture was thoroughly stirred by a magnetic mixer at 80–90°C to form a transparent solution (A). The Ti(O–Bu)$_4$ was added to the remaining molten stearic acid while stirring to form a transparent solution (B). Then (A) and (B) were mixed together with vigorous stirring. After 2 h, a homogenous transparent solution was formed. The solution was ignited in air and the obtained powders were calcined at different temperatures ranging from 450 to 900°C for 2.5 h in air.

For comparison, the TiO_2/SnO_2 samples were also prepared by the conventional sol–gel method according to the procedure in Ref. (5). The molar ratio of the reactants was: Ti(O–Bu)$_4$: H_2O:EtOH:HCl:$SnCl_4 \cdot 5H_2O = 1:4:15:0.3:r$ ($r = 0$, 0.05, 0.10, 0.15, 0.20, 0.25). Ti(O–Bu)$_4$ was diluted with half the prescribed amount of ethanol at first, into which $SnCl_4 \cdot 5H_2O$ was added, and this mixture was stirred thoroughly by a magnetic mixer. Then, H_2O and HCl dissolved in the remaining ethanol were added dropwise to the solution above with continuous stirring to form homogenous sol. After storing at room temperature for some time, the sol was changed to a transparent orange gel. The gels were dried in a vacuum (10^{-1} Pa) furnace at 60°C for 6 h and then calcined at 500°C for 2.5 h in air.

The preparative process of SAM was monitored by FT-IR spectroscopy with a Bruker Vector22 spectrometer. The crystalline phase structures of these powders were investigated by the XRD measurement on a Bruker D8 ADVANCE X-ray diffractometer (Cu$K\alpha$ 0.15405 nm). For comparison of the crystallinity of different samples, identical amounts of samples were used for XRD measurement. The average grain sizes of these powders were measured by the XRD line profile analysis using Scherrer equation (24) and TEM observations on an H-800 transmission electron microscope. The specific surface areas of the calcined powders were analyzed using a BET surface analyzer (ASAP 2010, Micromeritics) and the content of rutile phase (X_R) in TiO_2 crystallines was calculated according to the following equation (25):

$$X_R = \frac{I_R/(I_A K)}{1 + I_R/(I_A K)},$$

where I_R is the height or area of the main peak of rutile phase in XRD pattern, while I_A is that of anatase phase, and K is a constant equal to 0.79.

The photocatalytic activities of the samples were evaluated by methyl orange decomposition under UV irradiation. Methyl orange was selected because of its simple chemical structure and good resistance to light degradation, which makes its quantification easy (26). The irradiation was provided by a 300 W high-pressure mercury lamp with a wavelength centered at 365 nm. The initial concentration of methyl orange in a quartz reaction vessel was fixed at approximately 20 mg L^{-1} with as-prepared catalysts loading of 0.5 g L^{-1}. The reaction cell (450 mL) was bubbled with air at a flow rate of 40 mL min^{-1}. The extent of methyl orange decomposition was determined by measuring the absorbance value at 465 nm using UV-1100 UV–Vis spectrometer. For comparison, the results were compared with the P25 powders available from Degussa A. G. (7).

RESULTS AND DISCUSSION

Characterization of Preparative Process

Stearic acid is one of the widely used surfactants. Its carboxylic acid group and long carbon chain endow it with strong ability to disperse various substances. We previously found that different metallic ions could be dispersed at molecular level in melted stearic acid and each component was uniformly mixed even in the resulting mixture after removing organic substance by combustion (21–23). In the preparation of TiO_2/SnO_2, strong chemical interaction existed between metal precursors and stearic acid. After $SnCl_4 \cdot 5H_2O$ was added into stearic acid [solution (A)], the characteristic absorption bands of –COOH (1704 and 943 cm^{-1}) decreased while a new band at 1542 cm^{-1} is observed, which is assigned to the stretching vibration of $-COO^-$ (see Fig. 1), indicating that stannic stearate was

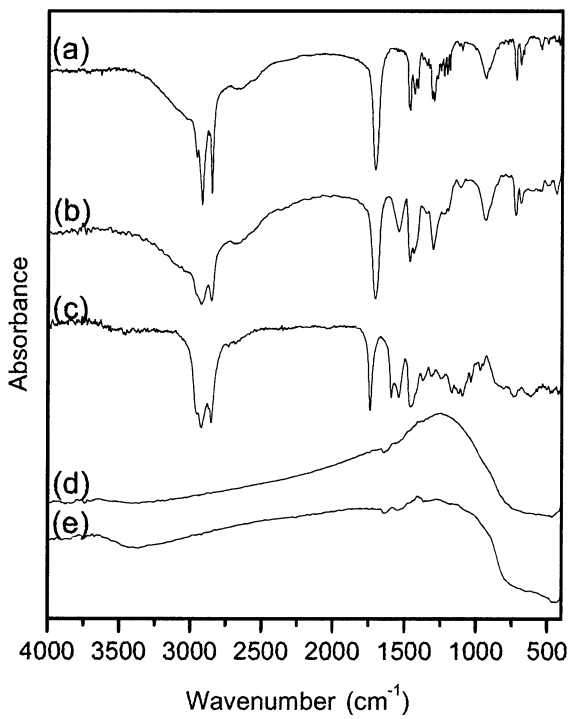

FIG. 1. FT-IR spectra of (a) stearic acid, (b) gel of $SnCl_4 \cdot 5H_2O$ in stearic acid (solution A), (c) gel of Ti(O-Bu)$_4$ in stearic acid (solution B), (d) TiO_2/SnO_2 ($r = 0.15$) powders calcined at 500°C (SAM), and (e) TiO_2/SnO_2 ($r = 0.15$) powders calcined at 500°C (sol–gel).

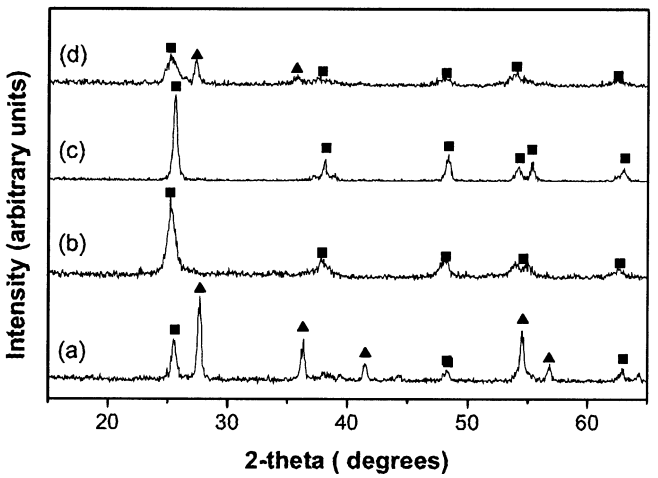

FIG. 2. XRD patterns of TiO_2/SnO_2 powders calcined at 500°C: (a) SAM $r = 0$, (b) SAM $r = 0.15$, (c) sol–gel $r = 0$, (d) sol–gel $r = 0.15$ (■: anatase ▲: rutile).

TABLE 1
XRD Experimental Results of Nanostructured TiO_2/SnO_3 Binary Oxide Powders (Calcined at 500°C) Prepared by SAM and Sol–Gel Method, Respectively

	SAM			Sol–gel			
r	X_R	D (nm)	Intensity (cps)	X_R	D (nm)	Intensity (cps)	Gelation time (day)
0	0.718	23.9	566.0	0	15.87	553.9	4
0.05	0	14.07	433.6	0.419	14.73	233.8	6
0.10	0	10.57	479.3	0.416	9.8	260.0	20
0.15	0	12.38	505.4	0.500	9.6	214.0	28
0.20	0	10.36	429.1	0.507	9.02	207.2	35
0.25	0	12.98	460.2	0.559	8.7	157.9	39

Note. D—average grain size calculated by the Scherrer equation; intensity—the relative intensity of the strongest peak of anatase phase at $2\theta = 25.3°$.

formed. After $Ti(O\text{-}Bu)_4$ was added into stearic acid [solution (B)], two new bands at 1590 and 1540 cm^{-1} appeared and the band at 1457 cm^{-1} strengthened. The bands at 1430–1470 and 1550–1590 cm^{-1} were attributed to COO^- stretching vibration for bidentate of Ti(IV)–carboxylic acid complex (27), indicating that a strong coordination interaction between Ti(IV) and stearic acid existed. Through the strong interaction between metal elements and stearic acid, Ti(IV) and Sn^{4+} were uniformly dispersed in the stearic acid, attaining molecular level distribution.

In SAM, stearic acid was excessive, there was appropriate 30% stearic acid had no direct interaction between metallic ions, which may function as dispersant in the system. In addition, the mixing process is performed at melted state, i.e., liquid state. Therefore, metallic ions were well dispersed and separated by stearic acid in this mixing system. The highly dispersed precursor guaranteed uniformity of the resulted TiO_2/SnO_2 powders.

Microstructure of Nanocrystalline TiO_2/SnO_2

Figure 2 shows the XRD patterns of TiO_2/SnO_2 ($r = 0$ and 0.15, 500°C) powders prepared by SAM and sol–gel method, respectively. In the sol–gel method, the crystal phase of pure TiO_2 is anatase, while the rutile phase appeared in TiO_2/SnO_2 samples at the same calcination temperature (also see Table 1), indicating that SnO_2 promoted the $A \rightarrow R$ transformation of TiO_2 in sol–gel method. This is in agreement with the results in Ref. (5).

However, for SAM, the rutile phase existed in pure TiO_2 and no rutile phase was detected when TiO_2 was coupled with SnO_2. The influence of the SnO_2 concentration on the $A \rightarrow R$ transformation in SAM is depicted in Fig. 3. It can be seen that with the increasing of the content of SnO_2, the increase of the X_R is reduced gradually, which suggests that the $A \rightarrow R$ transformation is delayed by the increase of SnO_2, i.e., the anatase phase is stabilized by the addition of SnO_2. This is completely contrary to the case in sol–gel method.

Furthermore, the crystallinity of the TiO_2/SnO_2 powders was affected by the preparative method as shown in Table 1. The addition of SnO_2 extensively decreased the X-ray intensity of anatase phase in sol–gel, but had little effect in SAM. In general, the crystallinity of powders prepared by SAM was higher than that prepared by sol–gel method.

Preparative methods also influenced the grain size and dispersity of the obtained powders. The average grain size of the obtained powders are listed in Table 1. Figure 4 shows the TEM micrographs of TiO_2/SnO_2 ($r = 0.15$) powders prepared by both SAM and sol–gel method calcined at

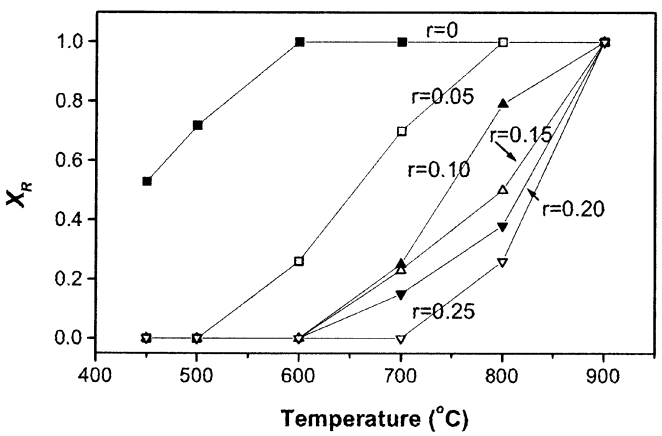

FIG. 3. Content of rutile phase (X_R) in nanostructured TiO_2/SnO_2 binary oxides prepared by SAM with different r values.

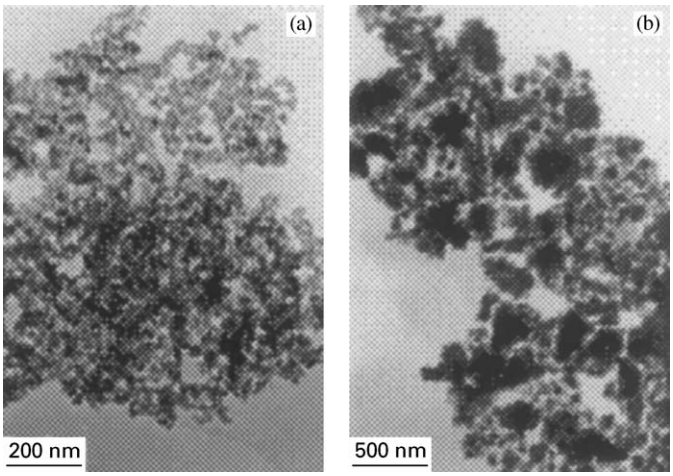

FIG. 4. TEM micrographs of TiO_2/SnO_2 ($r = 0.15$) prepared by (a) SAM, and (b) sol–gel method calcined at 500°C.

500°C. The average grain size of TiO_2/SnO_2 powders prepared by SAM is about 15 nm, which is little larger than that of sol–gel method (ca. 10 nm). But the powders obtained by SAM showed better dispersity. The difference of dispersity may result from the difference of the amount of surface hydroxyls. The surface hydroxyl of oxides was considered to be one of the main reasons to drive the aggregation of grains due to the hydrogen bonding between these hydroxyls (28). The surface of the powders obtained by sol–gel was rich in hydroxyl as a result of hydrolysis (29). But as for the powders resulted from SAM, the surface hydroxyl was scarce because the preparative process was nonhydrolytic. This fact is confirmed by the FT-IR spectra of the newly prepared products that the observed characteristic band of hydroxyl at about $3400\,cm^{-1}$ was stronger in Fig. 1e than that in Fig. 1d.

Our preliminary experiments show that the porous structure and the specific surface area of the products are also related to the preparative methods. The powders ($r = 0.15$) prepared by the SAM exhibits a higher surface area of $112.4\,m^2\,g^{-1}$, while the powders ($r = 0.15$) resulted from sol–gel method shows a lower surface area of $71.7\,m^2\,g^{-1}$. Figure 5 shows the nitrogen adsorption/desorption isotherms of the two samples at liquid nitrogen temperature. According to the IUPAC classification, the isotherm profile of sample prepared by SAM was classified as type III, and the profile of sol–gel method was classified as type IV. The completely different isotherm profiles of the two samples indicated the difference of the microporous structure between them.

At the present time, we are not sure of the mechanism causing the difference of the microstructure of TiO_2/SnO_2 nanocrystallines prepared by different methods. Possibly, it mainly originates from the different formation process of nanocrystallines in different methods. Nanocrystalline TiO_2/SnO_2 binary oxides are formed through a hydrolysis process in the sol–gel route, while the SAM route is a nonhydrolytic process.

Photocatalysis of Nanocrystalline TiO_2/SnO_2

Figure 6 shows the absorption spectra of an aqueous solution of methyl orange decomposed by TiO_2/SnO_2 ($r = 0.15$, 500°C) prepared by SAM. The obvious decrease of absorption peaks both in visible and ultraviolet regions with irradiation time indicates that the methyl orange solution can be degraded by photocatalysis and $20\,mg\,L^{-1}$ methyl orange can be almost completely decomposed in 12 min by using TiO_2/SnO_2 ($r = 0.15$, SAM).

The influence of the concentration of SnO_2 on the photocatalytic activity of the prepared TiO_2/SnO_2 is shown in Fig. 7. For samples prepared by sol–gel method, the degradation rate of methyl orange was decreased by the addition of SnO_2 as shown in Fig. 7a. The crystal phase transformation of the addition of SnO_2 accounts for this result. Although the addition of SnO_2 may suppress the recombination of photoinduced electron–hole pairs and improve the photocatalytic activity (14–16), the samples ($r > 0$) prepared by sol–gel method calcined at 500°C contain

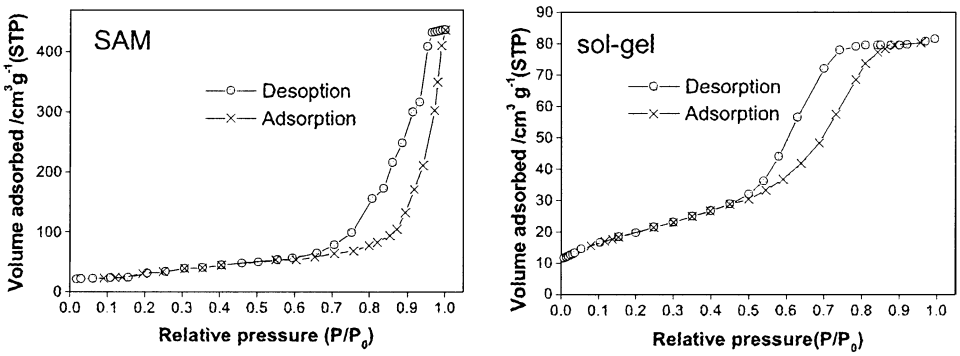

FIG. 5. Nitrogen adsorption–desorption isotherms of TiO_2/SnO_2 ($r = 0.15$) calcined at 500°C.

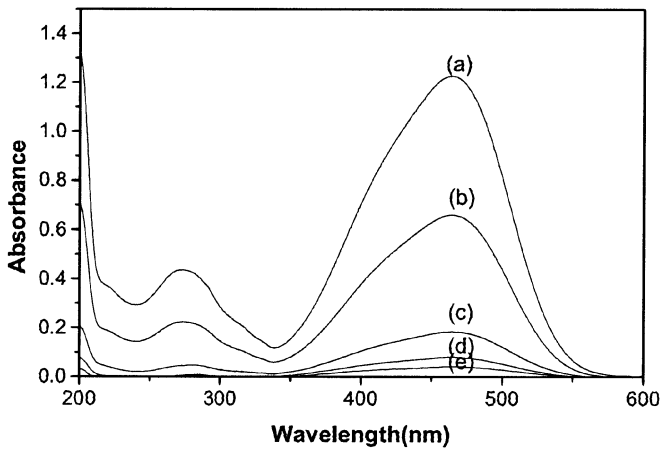

FIG. 6. Absorption spectra of methyl orange solution ($20\,mg\,L^{-1}$) photocatalyzed by TiO_2/SnO_2 (SAM, $r = 0.15$, $0.5\,g\,L^{-1}$) with different intervals: (a) 0 min, (b) 3 min, (c) 6 min, (d) 9 min, and (e) 12 min.

a considerable amount of rutile-type TiO_2, whose photocatalytic activity is much lower than that of anatase (6, 7).

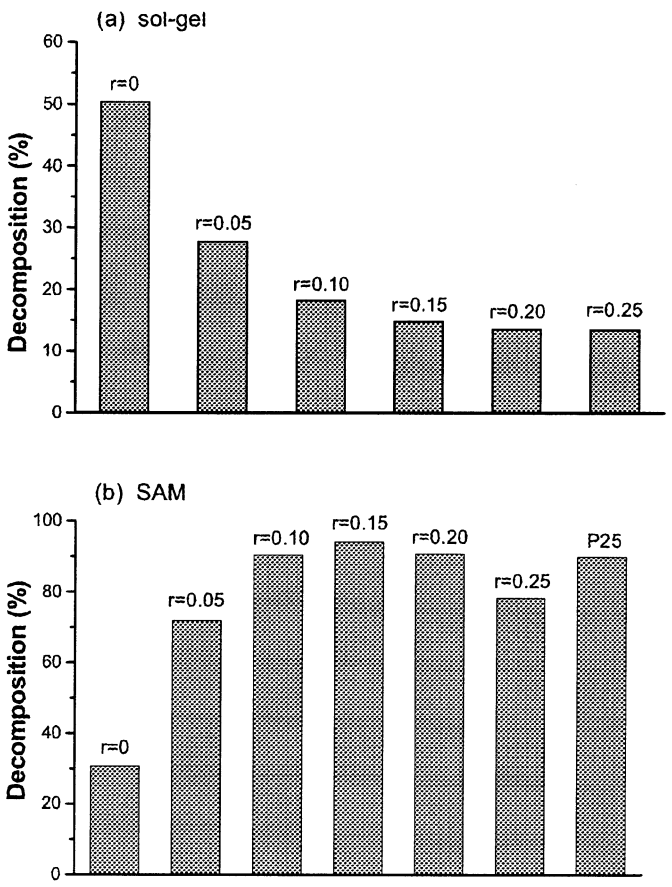

FIG. 7. Photodegraded amounts of methyl orange by the TiO_2/SnO_2 binary oxides (calcined at 500°C) and *P*25 after 12 min irradiation.

However, the photocatalytic activity of the samples prepared by SAM was increased with increasing the content of SnO_2 in the case of $r \leq 0.15$ and decreased as $r > 0.15$ (Fig. 7b). The highest degradation rate was reached by using TiO_2/SnO_2 ($r = 0.15$), which was even higher than that of *P*25 and nearly twice as that of TiO_2/SnO_2 ($r = 0$) obtained by sol–gel method. The excellent photocatalytic activity should be attributed to its high specific surface area, good dispersity, anatase structure and also the sensitization of coupling SnO_2.

Another advantage of SAM is that this method is very convenient and rapid, which is very important for industrial application. In our experiment, samples with any concentration of SnO_2 can be obtained within 5 h by SAM. While in sol–gel method, depending on the concentration of SnO_2, the gelation time increases with increasing the SnO_2 concentration from 4 to 39 days as shown in Table 1.

CONCLUSIONS

TiO_2/SnO_2 nanocrystalline powders with good dispersity, high crystallinity and large specific surface area were successfully prepared by SAM. The anatase structure of TiO_2 was stabilized by the addition of SnO_2 and the prepared TiO_2/SnO_2 showed high photocatalytic activity in the photoinduced degradation of methyl orange.

ACKNOWLEDGMENTS

The authors thank the Doctoral and Postdoctoral Science Foundations of Department of Education of China and Natural Science Foundation of Jiangsu province for financial support.

REFERENCES

1. N. I. Al-salim, S. A. Bagshaw, A. Bittar, T. Kemmitt, A. J. McQuillan, A. M. Mills, and M. J. Ryan, *J. Mater. Chem.* **10,** 2358 (2000).
2. T. A. Konovalova and L. D. Kispert, *J. Phys. Chem. B* **103,** 4672 (1999).
3. M. Iwasaki, M. Hara, H. Kawada, H. Tada, and S. Ito, *J. Colloid Interface Sci.* **224,** 202 (2000).
4. S. Ito, S. Inoue, H. Kawada, M. Hara, M. Iwaski, and H. Tada, *J. Colloid Interface Sci.* **216,** 59 (1999).
5. X. Z. Ding and X. H. Liu, *Mater. Sci. Eng. A* **224,** 210 (1997).
6. J. Moon, H. Takagi, Y. Fujishiro, and M. Awano, *J. Mater. Sci.* **36,** 949 (2001).
7. J. Ovenstone, *J. Mater. Sci.* **36,** 1325 (2001).
8. L. Spanhel, H. Weller, and A. Hengiein, *J. Am. Chem. Soc.* **109,** 6632 (1987).
9. K. R. Gopidads, M. Bohorquez, and P. V. Kamat, *J. Phys. Chem.* **94,** 6435 (1990).
10. N. Serpone, E. Borgarello, and M. Grätzel, *J. Chem. Soc., Chem. Commun.* 342 (1984).
11. S. Hotchandant and P. V. Kamat, *J. Phys. Chem.* **96,** 6834 (1992).
12. T. Sato, K. Masaki, K. Sato, Y. Fujishiro, and A. Okuwaki, *Chem. Tech. Biotechnol.* **67,** 339 (1996).
13. M. Machida, X. W. Ma, H. Taniguchi, J. Yabunaka, and T. Kijima, *J. Mole. Catal. A: Chem.* **155,** 131 (2000).

14. I. Bedja and P. V. Kamat, *J. Phys. Chem.* **99,** 9182 (1995).
15. A. Vinodgopal and P. V. Kamat, *Environ. Sci. Technol.* **29,** 841 (1995).
16. Y. A. Cao, X. T. Zhang, W. S. Yang, H. Du, Y. B. Bai, T. J. Li, and J. N. Yao, *Chem. Mater.* **12,** 3445 (2000).
17. M. H. Selle, J. Sjöblom, and R. Lindberg, *Colloid Polym. Sci.* **273,** 951 (1995).
18. Z. F. Liu and R. J. Davis, *J. Phys. Chem.* **98,** 1253 (1994).
19. J. A. Montoya, P. Angel, and T. Viveros, *J. Mater. Chem.* **11,** 944 (2001).
20. M. P. Coles, C. G. Lugmair, K. W. Terry, and D. Tilley, *Chem. Mater.* **12,** 122 (2000)
21. G. Xiong, X. J. Yang, L. D. Lu, and X. Wang, *J. Mater. Sci* **35,** 931 (2000)
22. X. H. Wang, D. Li, L. D. Lu, and X. Wang, *J. Alloys Compd.* **237,** 45 (1996).
23. G. Xiong, Z. H. Mai, S. L. Cui, Z. X. Ni, X. Wang, and L. D. Lu, *Chem. Mater.* **13,** 1943 (2001).
24. L. S. Birks and H. Frienman, *J. Appl. Phys.* **17,** 687 (1946).
25. R. Debnath and J. Chaudhuri, *J. Mater. Res.* **187,** 79 (1991).
26. G. T. Brown and J. R. Darwent, *J. Phys. Chem.* **88,** 4955 (1984).
27. Y. Murasami, T. Matsumoto, and Y. Takasu, *J. Phys. Chem. B* **101,** 1836 (1997).
28. N. L. Wu, S. Y. Wang, and I. A. Rusakova, *Science* **285,** 1375 (1999).
29. T. J. Trentler, T. E. Denler, J. F. Nertone, A. Agrawal, and V. L. Colvin, *J. Am. Chem. Soc.* **121,** 1613 (1999).